Langmuir

ARTICLE

pubs.acs.org/Langmuir

Nanocontact Electrification: Patterned Surface Charges Affecting Adhesion, Transfer, and Printing

Jesse J. Cole, Chad R. Barry, Robert J. Knuesel, Xinyu Wang, and Heiko O. Jacobs*

Department of Electrical and Computer Engineering, University of Minnesota, 200 Union Street SE, Minneapolis, Minnesota 55455, United States

Supporting Information

ABSTRACT: Contact electrification creates an invisible mark, overlooked and often undetected by conventional surface spectroscopic measurements. It impacts our daily lives macroscopically during electrostatic discharge and is equally relevant on the nanoscale in areas such as soft lithography, transfer, and printing. This report describes a new conceptual approach to studying and utilizing contact electrification beyond prior surface force apparatus and point-contact implementations. Instead of a single point contact, our process studies nanocontact electrification that occurs between multiple nanocontacts of different sizes and shapes that can be formed using flexible materials, in particular, surface-functionalized poly(dimethylsiloxane) (PDMS) stamps and other common dielectrics (PMMA, SU-8, PS, PAA, and SiO_2). Upon the formation of conformal contacts and forced delamination, contacted regions become charged, which is directly observed using Kelvin probe force microscopy revealing images of charge with sub-100-nm lateral resolution. The experiments reveal chemically driven interfacial proton exchange as the dominant charging mechanism for the materials that have been investigated so far. The recorded levels of uncompensated charges approach the theoretical limit that is set by the dielectric breakdown strength of the air gap that forms as the surfaces are delaminated. The macroscopic presence of the charges is recorded using force−distance curve measurements involving a balance and a micromanipulator to control the distance between the delaminated objects. Coulomb attraction between the delaminated surfaces reaches 150 N/m^2. At such a magnitude, the force finds many applications. We demonstrate the utility of printed charges in the fields of (i) nanoxerography and (ii) nanotransfer printing whereby the smallest objects are ∼10 nm in diameter and the largest objects are in the millimeter to centimeter range. The printed charges are also shown to affect the electronic properties of contacted surfaces. For example, in the case of a silicon-on-insulator field effect transistors are in contact with PDMS and subsequent delamination leads to threshold voltage shifts that exceed 500 mV.

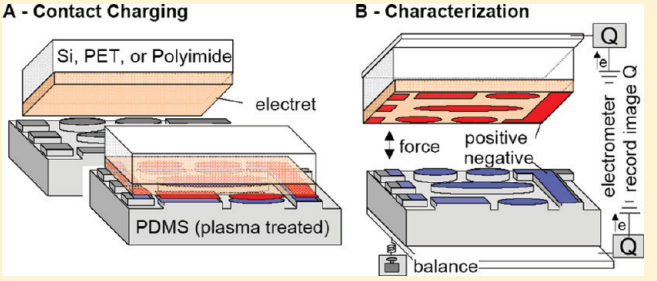

The basic phenomenon of electrification by contact is well known and can be attributed to three fundamental processes: material transfer, ion transfer, and electron transfer. Electron transfer dominates if at least one of the materials is a semiconductor or a metal with free electrons.[1] If both materials are insulators, then the fundamental charge-transfer mechanism cannot be explained on the basis of electronegativity alone and requires the consideration of the chemical nature of all functional groups.[2] This becomes increasingly complicated if polymeric insulators are used. In all cases, contact electrification leads to uncompensated surface charges that impact the force of adhesion. For example, surface force apparatus measurements by Horn et al.[3] demonstrated that the electrostatic force of adhesion between crossed insulating cylinders can exceed 6 J/m^2, which is comparable to the fracture energies of covalently bonded materials. We note that the reported values[3] were exceptionally large, exceeding anything that had been reported before and perhaps possible considering the breakdown strength of air. Considering the context of soft lithography,[4] nanoimprint lithography, and nanotransfer printing,[5] the formation and fracture of conformal contacts have become mainstream and are no longer limited to single point contacts. This enables a new set of investigations into the fundamental science and applications of contact electrification over extended surfaces using multiple contacts of different sizes and shapes.

As a first step in this direction, we report on controlled delamination experiments between poly(dimethylsiloxane) (PDMS) and other common dielectrics to quantify and monitor charge transfer and the subsequent electrostatic force of adhesion. In addition to the commonly used tables of electronegativity, we identified that proton exchange reactions established in solution chemistry provide the best approach to explaining interfacial charging between the dielectrics that we have investigated so far. The dielectrics include poly(methyl methacrylate) (PMMA), epoxy photoresist (SU-8), polystyrene (PS), poly(acrylic acid) (PAA), and silicon oxide (SiO_2). The magnitude of

Received: February 28, 2011
Revised: April 8, 2011
Published: April 28, 2011

ACS Publications © 2011 American Chemical Society

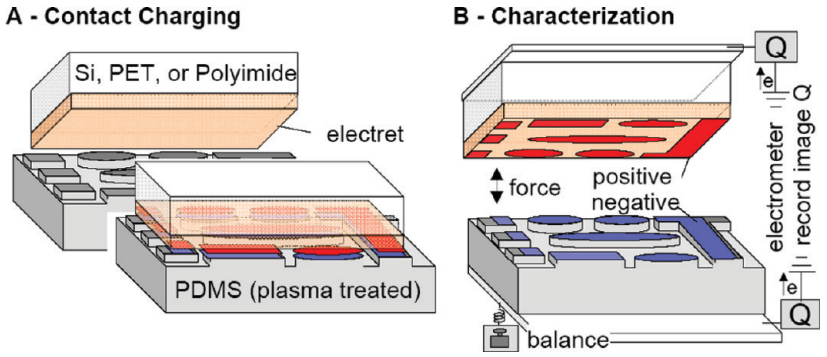

Figure 1. Contact electrification process and measuring procedure. (A) A dielectric coated substrate is placed in contact with an oxygen-plasma-treated, patterned PDMS stamp. Charge transfer occurs in the areas of contact between both materials. (B) An electrometer records the quantity of accumulated image charges on metallic plates holding both the substrate and stamp. A connected balance records the weight reduction of the stamp as the charged substrate is separated, and then again during reapproach. (See Figure S1 for a photograph of the actual implementation.)

electrification can be adjusted through surface functionalization of the PDMS and reach values close to the physical limit near the dielectric breakdown strength of air. The uncompensated charges yield a long-range electrostatic attractive force of 150 N/m^2. Corresponding force−distance curves show a phenomenological relationship between long- and short-range attractive forces where a controlled increase in the recorded long-range electrostatic force equates to a stronger short-range adhesion. The gained knowledge finds several applications: in the context of laterally confined charge patterning with sub-100-nm lateral resolution, it extends previously reported serial scanning probe[6] and electric nanocontact charging techniques because it can pattern samples that are at least 100 times larger than what has been reported while maintaining the same high lateral resolution. Moreover, previous[6−10] charging processes required a conducting substrate underneath the dielectric. The reported process eliminates this requirement as well as the requirement that an external voltage has to be applied to the sandwiched structures to inject and transfer charge at the interface. In the context of nanoxerography, it is demonstrated that the chemically driven charge-patterned surfaces prepared by nanocontact electrification can be developed into visible patterns using the charge-directed deposition of nanoparticles. In the context of transfer printing, it is demonstrated that the strong adhesive forces that stem from uncompensated surface charges can be used to transfer semiconducting components from one substrate to another whereby the size of the components can span 3 orders of magnitude. Finally, in the context of printable electronics it is demonstrated that a contact with PDMS leads to high levels of uncompensated surface charge, which affects transport in nearby semiconducting device layers and is measured in terms of transistor threshold voltage shifts that exceed 500 mV in the MOSFET devices that have been tested. Threshold voltage shifts were found to depend on the covering material such that the threshold voltage was adjusted positively (or negatively) after contacting SiO_2 (or PMMA) covering the n-channel FET.

Figure 1 illustrates the basic nanocontact electrification measurement procedure. PDMS was chosen as the primary contacting material because of its wide use in today's scientific world. For lateral charge-patterning experiments, PDMS stamps were prepared with raised posts through molding[7,8] that provides small contact areas alongside an unchanged reference. For transfer experiments, we left the surface flat and unpatterned. To investigate the transfer of charge, electret-coated chips (PMMA, SU-8, PS, PAA, and SiO_2) with film thicknesses of around 100−200 nm[11] were placed onto the PDMS stamps and left in contact for 1 min before forced delamination. Untreated PDMS substrates left residues on the contacted surfaces and did not provide reproducible results. To clean and activate the PDMS surface, we used a pure oxygen plasma etcher (SPI Plasma Prep II) operating at 80−100 W at 10 Torr for 40 s. This process is commonly used because it creates an energetic, hydrophilic surface that reduces the transfer of uncured material during contact when compared to untreated PDMS.[12−15]

To quantify the level of contact electrification as a result of forced delamination, we analyzed all samples using Kelvin probe force microscopy (KFM) immediately after cleavage. KFM records the surface potential distribution and provides a direct measure of the amount of electrification with respect to areas that have not been contacted.[16] Although the level and polarity varied, localized electrification is observed at high levels after conformal contacts are delaminated. During the formation and delamination process, no lateral frictional forces or sliding motion was applied, which is different from other more classical implementations also aimed at producing high levels of uncompensated charge. Figure 2A,B illustrates the associative effect of the electret material, in this case PMMA versus SiO_2, on the polarity of the produced patterns. Specifically, PMMA charged positively at contacted areas and SiO_2 charged negatively. Figure 2C,D reveals the effect of plasma treatment of the PDMS on the charge concentration. Without plasma activation (Figure 2C), the highest level of charge was at least a factor of 4 smaller than that achieved by contacting the samples with plasma-treated stamps (Figure 2A,B,D,G,H).

The illustrated nanocontact electrification process could in principle be attributed to a number of factors including material transfer. To determine if substantial material transfer is required and involved, we conducted several AFM topography measurement and X-ray photon spectroscopy (XPS) studies. We found that no substantial material transfer is required to cause charging as shown in Figures S2 and S3. For example, no measurable material transfer after contact between plasma-treated PDMS and untreated PMMA was recorded, which is consistent with prior XPS studies done by Uhrich et al.[15,17] However, high levels of contact electrification were observed for this interface as shown in Figure 2D, which means that the charging cannot be explained by simple material transfer. Because a measurable amount of material transfer (i.e., more than a single monolayer) is not required, the process must be dominated by small molecular changes such as interfacial ion or electron transfer.

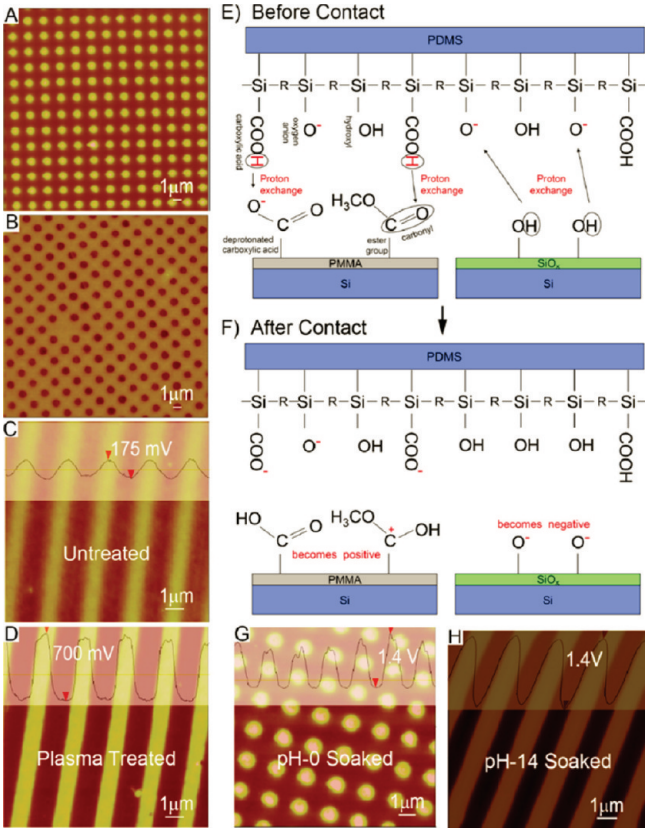

Figure 2. KFM contact electrification results, charge-transfer theory, and control experiments. (A–D) KFM images of 1 μm pitched dot- and line-type patterns showing the influence of material and plasma treatment on the polarity and charge concentration. (A) PMMA charged positively and (B) SiO_2 charged negatively upon contact with the same plasma-activated PDMS stamp.(C, D) Plasma treatment of the PDMS yields a 4-fold increase in the surface charge on PMMA. (E, F) Proposed proton exchange reaction between plasma-treated PDMS and both PMMA and SiO_2. In the case of PMMA, hydrogen protons dissociate from the PDMS surface and attach to a deprotonated carboxylic acid or carbonyl site within the ester groups on the PMMA surface. The situation is reversed for SiO_2 because of the abundance of hydroxyl groups on the SiO_2 surface. (G, H) KFM control experiments to enhance charge transfer by pH surface treatment of the PDMS stamp prior to contact. (G) pH 0 treatment increases the positive surface charge on PMMA, and (H) pH 14 treatment increases the negative surface charge on SiO_2.

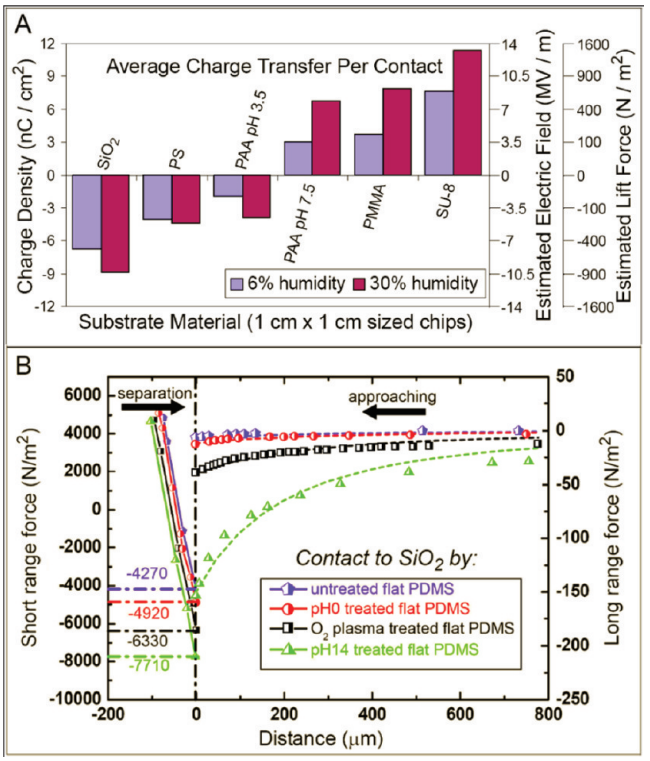

Figure 3. Recorded charge levels on various materials and resulting short- and long-range force. (A) Average Faraday cup electrometer recordings at 6 and 30% relative humidity for six different electret materials after contact electrification with oxygen-plasma-treated PDMS. Electric field and adhesive force values estimated from the charge density measurements are also displayed. (B) Force–distance curves have two regimes that describe the force–distance relationship up to the point of separation (left, short-range) and during reapproach (right, long-range). The curves show untreated, pH 0-treated, oxygen-plasma-treated, and pH 14-treated PDMS that is brought into contact with SiO_2. The long-range force–distance curves follow a stray capacitance model (dashed lines) that considers the coupling of the printed charges to nearby conducting surfaces that reduce the attractive force as the separation is increased.

The working hypothesis of the charging mechanism for the materials studied is illustrated in Figure 2E,F and involves hydrogen proton exchange reactions at the interface similar to acid–base reactions in solution chemistry. Although we limit our discussion to PMMA and SiO_2, the other tested materials follow the same general theme: chemically driven proton exchange more suitably explains the observed results than looking at the macroscopic electronegativity alone. In this case, plasma treatment attacks the Si–CH_3 bonds on the surface of the PDMS, leaving very reactive silyl radicals that capture O, OH, COOH, and oxygen radicals, forming a mildly acidic and highly polar surface.[12,14] Many polymers, such as PMMA, contain polar end groups that can participate in ionic charging and interfacial reactions. The ester end group in PMMA for example is slightly positive. PMMA can also be considered to be less acidic than plasma-treated PDMS because it contains fewer surface hydrogen atoms. This creates a chemical potential difference that allows hydrogen protons to transfer during contact as illustrated in the schematic (left sides of Figure 2E,F). After separation (Figure 2F), the hydrogen atoms remain trapped on the PMMA surface, leaving these areas positively charged as observed in Figure 2A. In accordance with this hydrogen proton exchange reaction concept, silicon dioxide (right sides of Figure 2E,F) should yield the opposite polarity because the oxidized surface of the SiO_2 substrate has an abundance of hydroxyl groups making it more acidic than PDMS. The hydroxyl groups provide hydrogen ions to react with the oxygen ions on the PDMS, leaving a negative charge on the SiO_2 surface as observed in Figure 2B. In short, deprotonated PMMA accepts protons from PDMS and SiO_2 donates protons to PDMS.

We tested protonation/deprotonation further by loading PDMS with acids and bases. In the case of PMMA (proton acceptor), contact with a highly protonated PDMS stamp (referred to as pH 0-treated) increased the amount of positive charge transfer to PMMA (Figure 2G). In the case of SiO_2 (proton donor), contact with a highly deprotonated PDMS stamp (referred to as pH 14-treated) increased the amount of negative charge transfer to SiO_2 (Figure 2H). In these depicted results, we

soaked the stamps for 1 h in an acidic buffer solution of 1 M hydrochloric acid in water in one case (pH 0-treated) and in a basic solution of 1 M sodium hydroxide in water in the other (pH 14-treated). After removing the stamp from the pH solutions, we quickly (2 s) rinsed the surface with deionized water and then blew it dry with nitrogen. The rinsing of the pH 14-treated PDMS stamp removes any potential salt residues that would otherwise prevent the formation of uniform conformal contacts. Our interpretation of the observed increase in charging (Figure 2G,H) is that the 2 s rinsing step does not completely remove the level of protonation/deprotonation acquired during the 1 h pH soaking step of the permeable plasma-treated PDMS surface layer.

The recorded potential difference in KFM studies can be used as a first-order estimate of the trapped surface charge density. For example, a recorded 1.5 V potential difference (Figure 2G) for a 200-nm-thick PMMA film represents a charge density of ~10 nC/cm^2.[18] Faraday cup and force−distance measurements can also be used to confirm these values. The electrometers and microbalance shown in Figure 1B and the photograph in Figure S1 were added to the experimental process to measure the amount of charge that is transferred at the interface and the subsequent electrostatic force of adhesion. In the electrometer arrangement, both stamps and substrates are placed onto metallic plates that act as Faraday cups that accumulate image charges that are equal but opposite in sign to the charge on the surface of the materials.[19]

Figure 3A provides a summary of the recorded charge levels for six different electret materials (SiO_2, PS, PAA at pH 3.5, PAA at pH 7.5, PMMA, and SU-8) contacted by plasma-treated PDMS at 6 and 30% relative humidity. Out of the six different electrets materials, SiO_2 charged the most negative and SU-8 the most positive. Poly(acrylic acid) (PAA, from Sigma-Aldrich) was used as an example where the polarity of charge transfer can be altered. Poly(acrylic acid) was originally purchased in a pH 7.5 formulation, and then the pH was adjusted to 3.5 by the addition of dilute hydrochloric acid as measured by a silver ion pH meter. We tested 100 nm of spin-coated PAA at a pH of 3.5, which predictably resulted in a negative charge on the PAA surface after contact with PDMS (Figure 3A); the more acidic PAA-3.5 has more hydrogen protons to donate to the PDMS, which means that contacted areas become negatively charged. In a second experiment, we reverse the contact charge polarity by using a poly(acrylic acid) thin film that was prepared using a PAA solution with an increased pH of 7.5. This can again be explained because the now deprotonated PAA-7.5 receives hydrogen protons from PDMS during contact, resulting in the acquired positive charge.

As shown in the chart (Figure 3A), the contact charging process depends on the relative humidity. Increasing the relative humidity from 6 to 30% increased the charge differential for all materials. The changes were not as dramatic outside the 6−30% window. This dependence again points toward charging that is driven by ion exchange rather than material or electron transfer; higher humidity will increase the amount of surface water that mediates the diffusion of ions across the interface as the chemically different surfaces are brought into contact. The chart also shows values for the estimated electric field strength, E, and estimated electrostatic force of adhesion, F, which can be directly calculated from the electrometer measurements using $E = \sigma/\varepsilon$ and $F = A\sigma^2/\varepsilon$, where A is the contact area, σ is the surface charge density, and ε is the permittivity of air. The calculated electric field strength based on the measured charge density ranged between 1 and 4 times the dielectric breakdown strength of air ($\sim 3 \times 10^6$ V/m) published for macroscopic electrodes. Interestingly, the values for the charge levels are very large but less than the levels record by Horn et al.[3] that imply even higher electric fields. We believe that the closeness to the breakdown strength of air in our case points to a self-limiting behavior. The closeness suggests that the upper level may be limited by partial discharge across the air gap as it forms; the existence of partial discharge has previously been reported.[3] In our case, the calculated electrostatic force of adhesion, $F = A\sigma^2/\varepsilon$, using the measured charge densities is estimated to exceed 500 N/m^2, providing a lift of 50 kg/m^2. This is a large force, and it should be possible to measure this directly using a balance. This was done by attaching the substrate chip to a balance/micromanipulator arrangement (Figures 1 and S1). This modified apparatus allows us to record force−distance curves.

Figure 3B shows the force−distance curves for SiO_2 substrates after contact with plasma-activated PDMS at ~30% relative humidity. The curves were recorded by measuring the microbalance weight reduction as a function of separation. The left side of the graph plots the overall adhesive force after contact up to separation whereas the right side of the graph plots the attractive Coulomb force as the substrate reapproaches the previously contacted PDMS. The graph shows a phenomenological relationship between short- and long-range forces. Such a phenomenological relationship has been observed before.[3] Specifically, high levels of short-range force (adhesion) correspond to a larger long-range force, but the short-range force is much larger in magnitude. The link has not yet been explained. A possible explanation is that for an ionically bonded surface, delamination results in the separation of ions. Not every ion is separated, and gas discharge always provides the upper limit to the level of remaining uncompensated ions and the long-range electrostatic force that can remain. A higher final concentration of uncompensated surface charge (and long-range forces) would imply that it originated from a higher initial concentration of ionic bonds (and short-range forces).

Surfaces treated to enhance the strength of the long-range electrostatic were harder to delaminate. The pH treatment resulted in an increase in both the short- and long-range forces for SiO_2 (Figure 3B, green triangles). The recorded long-range electrostatic force increased by a factor of 5 with a maximum value approaching 150 N/m^2, leading to an estimated field of $\sim 4.1 \times 10^6$ V/m using $E = \sigma/\varepsilon$. The value remains higher than the breakdown strength of air but is about a factor of 2 smaller than what we anticipated on the basis of the charge measurement alone (Figure 3A). Experimentally, it is a challenge to record the last data point at the smallest separation before the surfaces jump into conformal contact.

The recorded long-range electrostatic force in Figure 3 is a function of the separation distance between the contacted surfaces, which cannot be explained using a simple parallel plate model where the attractive force density is commonly calculated using $F/A = \sigma^2/2\varepsilon_0$, which is independent of distance. Instead, the recorded data fits a more accurate model that considers stray capacitances to nearby grounded plates that reduce the electric field in the air gap in between the charged layers as shown in Figure 4. After contact electrification, image charges $Q_i(d)$ are drawn from ground to flow to nearby metal plates. The amount of image charge $Q_i(d)$ increased as the separation d increases. To understand the rebalancing of charges and fields, it is important to consider how the capacitance changes as the air gap increases. For example, the capacitance across an increasingly large air gap

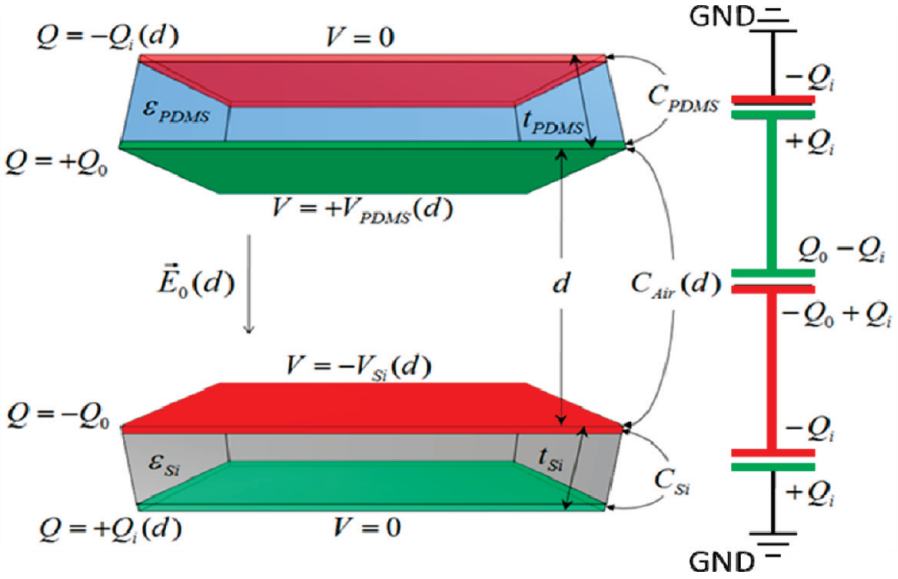

Figure 4. Electrode arrangement and coupling considering stray capacitance. Q_0 and $-Q_0$ represent the respective charge on the insulating PDMS (top green) and SiO_2 (bottom red) surface after contact electrification. Q_0 is fixed and not a function of the distance. Image charges Q_i are drawn into the conductive mounting plates, which alters the field distribution. The equivalent circuit model for the depicted capacitances is shown on the right. The total charge on the red and green plates remains Q_0. The value of Q_i depends on the separation d.

drops but the coupling capacitances to the grounded metal plates remains unchanged. Utilizing the grounded metal plates as a boundary condition with an electric potential of $V = 0$ and applying Kirchhoff's voltage law yields a relationship for the respective voltages $V_{air} = V_{PDMS} + V_{Si}$. Using $V_{air} = (Q_0 - Q_{i(d)})/C_{air(d)}$, $V_{PDMS} = Q_{i(d)}/C_{PDMS}$, and $V_{Si} = Q_{i(d)}/C_{Si}$, the equation expands to $(Q_0 - Q_{i(d)})/C_{air(d)} = Q_{i(d)}/C_{PDMS} + Q_{i(d)}/C_{Si}$, which yields the relationship for the image charges

$$Q_i(d) = \frac{Q_0}{1 + C_{air}/C_{PDMS} + C_{air}/C_{Si}} = \frac{Q_0}{1 + C_{air}/C_{stray}} \quad (1)$$

as well as the charges $Q_0 - Q_{i(d)}$ that couple the PDMS surface with the SiO_2 surface as the distance is increased:

$$Q_0 - Q_i(d) = \frac{Q_0}{1 + C_{stray}d/(\varepsilon_0 A)} \quad (2)$$

The previously introduced equation $F/A = \sigma^2/2\varepsilon_0 = Q^2/(2\varepsilon_0 A^2)$ can now be applied if we substitute Q with the relevant charge $Q_0 - Q_{i(d)}$, which is the charge that is responsible for the electric field and force that couples the PDMS surface to the SiO_2 surface. The substitution delivers the force per unit area as a function of separation d:

$$\frac{F_{air}}{A} = \frac{{\sigma_0}^2}{2\varepsilon_0} \frac{1}{(1 + C_{stray}d/(\varepsilon_0 A))^2} \quad (3)$$

Equation 3 provides an accurate model of the force−distance curves. For very small distances d, it approaches a constant value of ${\sigma_0}^2/2\varepsilon_0$, which represents the maximum force value that can be anticipated. At larger distances, the force drops inversely proportionally to the square of the distance. Equation 3 was used to fit the measured force−distance data (Figure 3B, dashed lines), which provides values of the actual stray capacitance of our system. The model represented by eq 3 is in good agreement with the experimental data.

Figure 5 shows that nanocontact electrification can be used to produce laterally confined charge patterns that can attract nanoparticles and large components. To give a qualitative comparison to prior parallel charge-patterning concepts,[7−10] nanocontact electrification provides a higher charge density with values close to the breakdown limit. The process provides an equally high lateral resolution but eliminates the need for fragile metallization on PDMS stamps that was previously required to produce conformal electrical contacts to inject charge by applying an external voltage. As a direct result, the areas are no longer limited to 1 cm^2; we have tested 100 cm^2 samples, observing uniform patterns in the tested areas. Other differences are that the use of an external bias voltage and a conducting substrate underneath the electret are also no longer required. In terms of the degradation of the charging ability of the PDMS as a function of use, we found that plasma-activated PDMS can be used multiple times before it needs reactivation; no measurable degradation was observed after 50 charging experiments. This observation can be explained if we compare a typical value of the recorded surface charge density with the intermolecular spacing of the reactive sites that are available; observed levels of charge of about 10 nC/cm^2 reflect about 1 elementary charge over a 40 nm × 40 nm area. This is a large spacing from a molecular standpoint. For example, the area per silynol group is estimated to be 0.7 nm × 0.7 nm. This leads to an abundance of surface groups on PDMS that can take part in the reaction and supports the observation that PDMS can be used multiple times. Plasma-activated PDMS, however, aged with time, losing most of its charging ability after 5 days. The aging can be linked to an earlier unrelated study[20] and involves the diffusion of oligomers over time from the bulk to the surface of the PDMS, returning it to its pretreated state.

The reported process impacts areas from the nanoscopic up to the macroscopic range. Figure 5A shows that the produced patterns of charge (left) can be develop into patterns of printed

dx.doi.org/10.1021/la200773x |*Langmuir* 2011, 27, 7321–7329

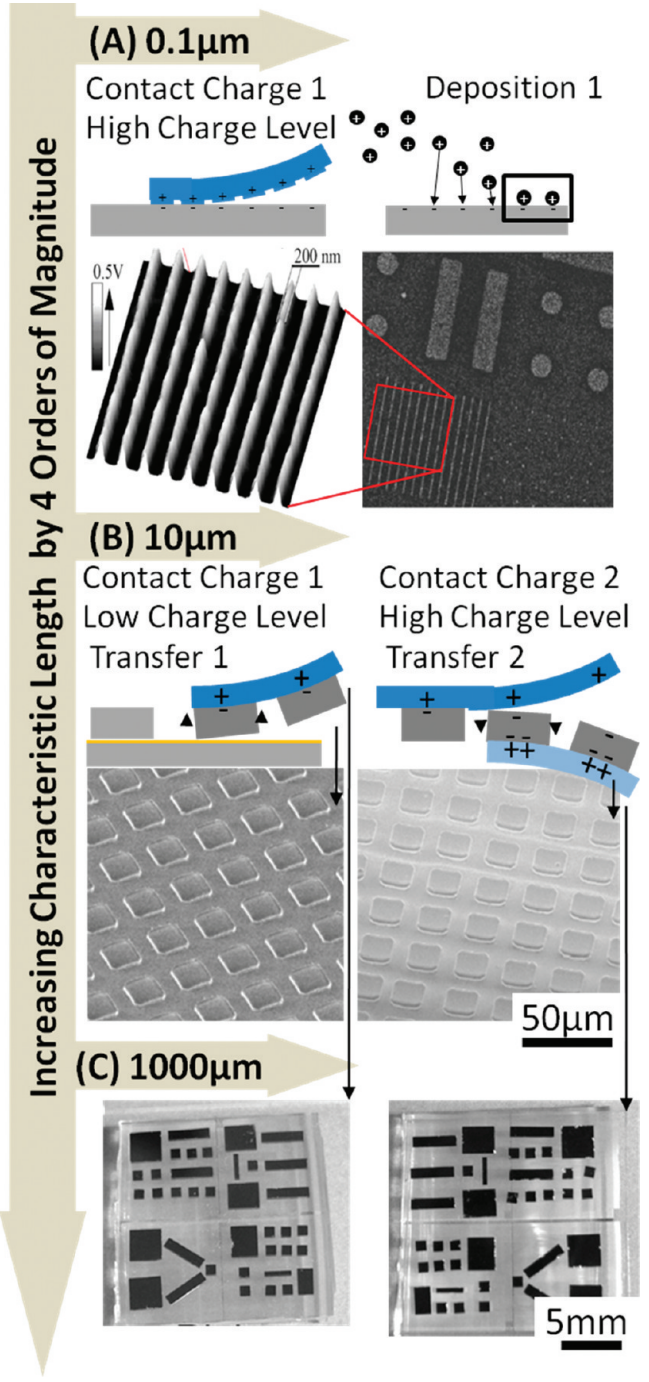

Figure 5. Implications of forces originating from uncompensated surface charges on objects spanning 4 orders of magnitude in size. (A) Charge pattern as recorded by KFM (left), which attracts 5−50 nm silver nanoparticles (right). (B, C) Two contact charging steps showing the selective transfer of micrometer- and millimeter-sized silicon chips from an initially rigid substrate onto pH0-treated PDMS (using a low interfacial charge level) and finally to pH14-treated PDMS (using a high interfacial charge level).

nanoparticles (right). In the given example, 5−50 nm silver nanoparticles were deposited directly from the gas phase using a previously reported nanomaterial source.[8,9] The strength of the effect is not limited to nanoscopic objects. Micrometer- and millimeter-sized objects can be transferred from one substrate to another by tailoring the electrostatic force of adhesion. For example, the adhesive forces exceeded the weight (1.6 g) of the 2 cm × 2 cm, 4-mm-thick PDMS stamps used in the experiments. After contact and separation, the stamp can be picked up on reapproach without bringing it into conformal contact. Figure 5B,C shows more practical examples in the area of flexible electronics that are selected on the basis of the discussed force−distance curves (Figure 3B). Silicon components with a native oxide were picked up from a donor wafer using an initial piece of PDMS (pH 0-treated, low interfacial charging) and subsequently transferred to another piece of PDMS (pH 14-treated, high interfacial charging) that showed the strongest force of adhesion. The components ranged in size from 1- to 5-mm-wide and 300-μm-thick silicon blocks (Figure 5B) to 20 μm × 20 μm Si chiplets that were 2 μm thick (Figure 5C). The components were picked up and transferred over a 2 cm × 2 cm area with yields of 100 and 99%, respectively.

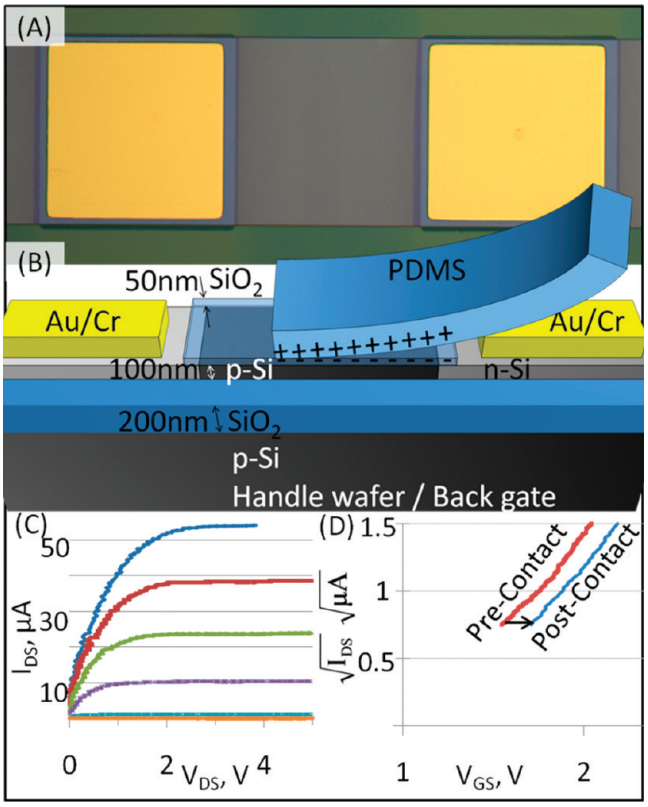

Figure 6. Contact electrification impacting the electrical performance of thin Si FETs. (A) Top-down optical microscope image next to a (B) cross-sectional schematic of the device. (C) I_{DS} vs V_{DS} curves showing the field-effect sensitivity to the back gate. (D) $I_{DS}^{1/2}$ vs V_{GS} plot showing the threshold voltage shift before and after contact and delamination.

Figure 6 shows that contact electrification by touching electronic devices with PDMS will affect the transport in nearby semiconducting device layers, which can be directly witnessed in terms of transistor threshold voltage shifts. The optical microscope image (Figure 6A) shows a thin silicon-on-insulator field-effect transistor (FET) that was used as a test structure. The device was fabricated using a commercially available silicon-on-insulator substrate where the thin, 100 nm silicon device layer was supported by 200 nm of buried silicon dioxide. Figure 6B shows a device schematic; full fabrication details are described in

the Methods section. The device layer of the FET was coated with SiO_2 or PMMA with respective negative or positive charging characteristics to observe if contact with PDMS would alter the threshold voltage. The I_{DS} vs V_{GS} transistor curves shown in Figure 6C were taken using the handle wafer as a back gate. We used the x-axis intercept of the $I_{DS}^{1/2}$ versus V_{GS} line to evaluate the threshold voltage that retains its accuracy even for added series resistances of SOI FETs.[21] For SiO_2, the threshold voltage applied to the back gate shifts to a higher voltage, which implies the presence of a negative surface charge on the SiO_2 surface. In other words, the presence of negative surface charges need to be compensated for by an extra positive gate voltage to turn ON the device. In the illustrated case (Figure 6D), we recorded ΔV_{th} = 127 mV for a d = 50 nm SiO_2 film, which leads to a charge density of $\sigma = -\varepsilon(\Delta V_{th}/d) = -8.78$ nC/cm^2 by modeling the surface potential as a floating body effect.[22] The sign and charge density agree very well with Figure 3A recorded values (a range of −7 to −9 nC/cm^2 was observed). For a 48 nm PMMA film, ΔV_{th} shifts negative by 60 mV, which indicates +2.76 nC/cm^2 of surface charge. Again, the polarity and magnitude are in good agreement. For PDMS in direct contact with a silicon n-FET with only its native oxide, the threshold voltage increased by 580 mV.

In conclusion, the cleavage of conformal contacts, which has become a common procedure in soft lithography and other soft-printing processes, typically leaves behind large amounts of surface charge as the surfaces are delaminated. Although these surface charges remain undetected with the most commonly applied spectroscopic measurement techniques including XPS and FTIR, direct evidence can be gained through Kelvin probe force microscopy and force−distance curve measurements. The recorded charging levels can be very high, and the upper levels seem to be self-limited by the dielectric breakdown strength of the air gap that forms as the materials are delaminated. The separated charges give rise to an electrostatic force of adhesion that can be detected over millimeter distances, exceeding 150 N/m^2 in some cases. The corresponding force−distance curves depict a phenomenological relationship between short- and long-range attractive forces. The presented explanation suggests a two-step process whereby the formation and delamination of interfaces bonded by ions precede contact electrification and the generation of long-range electrostatic forces. SiO_2, PS, PAA, PMMA, and SU-8 are all commonly used in the processing of semiconductor devices. We therefore expect that our findings will impact areas that go beyond the demonstrated charge-directed assembly and transfer applications. Charge printing is likely possible for other semiconductor substrates with a thin surface oxide including native oxides. For example, we found that the native oxide on Si is still prone to charging despite the fact that it is much thinner than the 160 nm thick thermal silicon oxide that was used in this study. The results reported here are especially meaningful in the context of soft lithography where PDMS contact with devices with thin oxides may result in altered threshold voltages. Specifically, the emerging field of printable and flexible electronics could be impacted, where contact printing methods and the delamination of interfaces are used to print and transfer materials. We anticipate that the presence of high levels of uncompensated charges may alter the functionality of various electronic devices including FETs unless models take these extra gate charges into account. The additional challenges are particularly relevant in the context of flexible electronics, where thin semiconductors, polymer insulators, and conformal contacts are widely employed.

METHODS

PDMS Fabrication and Surface Treatments. The PDMS fabrication for this study was unaltered from the commonly accepted technique. Specifically, we mixed 30 g of elastomer (Sylgard 184) and 3 g of curing agent (also Sylgard 184) for about 2 min at room temperature. Mixing caused gas bubbles to form, so uncured PDMS was degassed in a vacuum chamber at ∼30 Torr for 20 min. The uncured PDMS was poured onto silanized silicon and then degassed again for 1 h at ∼20 Torr. (The silicon may also be patterned with S1813 photoresist prior to treatment with octadecyltrichlorosilane if features were desired for the finished PDMS.) The degassed PDMS was cured in a convection oven at 60 °C for 12 h. The cured PDMS was inserted into a commercially available plasma cleaner (SPI, model Plasma Prep II) for oxygen plasma treatment. The system was purged with 99.99% oxygen, and then the 80−100 W, 13.56 MHz rf plasma was operated at 10 Torr for 40 s.

For pH treatment, cured PDMS was immersed in a high-molarity acid or base bath. The bath was contained in a high-density polymer (Nalgene) to minimize solvent−container reactions, and the bath was covered to minimize evaporation. We used 1 M HCl as a strong acid or 1 M NaOH as a strong base. Direct measurement of the solvent pH was performed with pH indicator paper that showed pH <1 and pH >13 for HCl and NaOH, respectively. Brief exposures of an electronic pH probe to the highly acidic and basic solutions also support these pH values. For ease of reference, we named the solutions pH 0 or pH 14. Cured PDMS pieces were soaked in one of these solutions for 1 h before use.

Electrometer Charge Measurement. When determining the quantity of transferred charge, we moved the PDMS at least 10 cm away to ensure that printed charges were electrostatically coupled only to the grounded metal mounting plate, which was in turn connected to the electrometer. The recorded level of uncompensated charge on the sample using the electrometer is fairly constant and drops only slightly over time at a rate that was less than 50 pC/min. The drop can be explained by the attraction of charged species from the environment. The electrometer measurements were conducted in a Faraday cage (shown in Supporting Information Figure S1), and the accuracy of the properly shielded instruments exceeded 1 pC (Keithley, model 6517). Most substrates were charged by at least 1 nC, which is well above the noise level of the instrument. Variations in recorded values between experiments, however, were found to be larger than the noise level and ranged from 20 to 300 pC. Variations in the recorded values repeating the same experiments cannot be considered to be a measurement error and are believed to be associated primarily with partial discharge by the attraction of gas ions from the gas environment, handling, time, and variations in the PDMS thickness that alter the coupling to the grounded metal plates that act as Faraday cups in the illustrated case. A fully automated system that takes the human interaction out of the loop and places the system inside a sealed environment to minimize airflow would allow a more accurate measurement. Such an improvement is not going to change the general trends found in this study.

Delamination Procedure. Separation of the PDMS was performed by pulling the PDMS stamp upward in a plane-parallel fashion. This leads to fast-moving delaminating fronts that break the conformal contact. Complete separation of the interface is estimated to be in the range of 50−500 ms. The plane-parallel separation occurs faster than conventional peeling and was chosen to minimize the risk of a partial discharge or arcing across the forming gap as a result of the high electric field that will be present at low separation distances. We have not observed the visual effects of arcing. We acknowledge, however, that there might be a dependency between the level of the recorded charge and the peel rate, which has not yet been investigated in detail. An approach to determine this relationship would be to use rolling cylinders with different roll speeds. Although viscoelastic effects are well known to play a role in the physical adhesion of PDMS to surfaces, we did not

observe that the peel rate has a strong affect on the level of charge transfer. Instead, the properties of PDMS and the material being contacted played much stronger roles, as reported here. Moreover, it would be interesting to control the environment beyond the humidity and, for example, perform measurements under vacuum or different gas environments to test if higher levels of charge are possible. This would provide further insight into the process that limits the amount of charge across the interface. Extending the present study in such a manner, however, would require the installation of a completely different apparatus.

Si Component Fabrication. The fabrication of the Si components involved the electron-beam deposition of Si onto Au-coated pillars of SU-8. Specifically, we first fabricated the SU-8 pillars on a ⟨100⟩ p-type 4 inch Si carrier substrate. The carrier substrate was cleaned for 15 min in a 120 °C piranha bath solution composed of 3:1 H_2SO_4 (99%)/H_2O_2 (30% in H_2O). The cleaned substrate was spin coated with Omnicoat (an SU-8 adhesion promoter) at a spinner speed of 2500 rpm for 30 s. The adhesion layer was baked on at 200 °C for 1 min. SU-8 was spin coated on top of the Omnicoat at 2500 rpm for 30 s and soft baked at 65 °C for 1 min and then at 95 °C for 2 min. SU-8 was soft contact exposed for 11 s under about 12 mW/cm^2 i-line illumination, subjected to a postexposure bake identical to the soft bake, and then developed for 4 min in PGMEA (propylene glycol monomethyl ether acetate). Excess Omnicoat was removed by exposure to 100 W, 100 mTorr oxygen plasma for 40 s. Using an electron-beam evaporator, 20 nm Cr and then 200 nm Au were deposited on the SU-8 pillars. Then 2 μm of Si was deposited by e-beam evaporation on top of the Au-coated SU-8.

The chemical bond of Si to the Au beneath is well known to be weak. Increasing the chemical adhesion of materials to Au typically requires an additional adhesion layer such as the Cr used on the SU-8 pillars. In the absence of an adhesion layer beneath the Si components, the Si components are easily delaminated from the Au and picked up by the weak electrostatic charge on the pH 0-treated PDMS. Following Si component pickup by PDMS, an optical microscope confirmed that the gold layer remained on the SU-8 pillars. The components then were transferred to a second piece of PDMS that was treated at pH 14.

Thin SOI MOSFET Fabrication. Fabricating charge-sensitive thin-SOI MOSFETs involved n-well doping, mesa etching, contact deposition, annealing, and insulator deposition. Each step used a pattern and etch-back process to avoid any debris that may be caused by liftoff processes. Beginning with 150-mm-diameter p-type Si on insulator wafers (SOITEC, inc.) with a 100 nm Si device layer on a 200 nm buried oxide, we deposited 300 nm of SiO_2 by PECVD at 340 °C. To define the dopant mask, the S1805 photoresist was photolithographically patterned and then given a 30 s oxygen plasma descum, and the underlying SiO_2 was etched in a 10:1 buffered oxide etch (a mix of HF and NH_4F in H_2O) for 150 s. The photoresist was removed by rinsing with acetone, methanol, and isopropyl alcohol. Phosphorus containing n-type spin-on dopant was spun on the wafer and then driven in by rapid thermal annealing at 900 °C for 10 s under a 6 s L/min flow of 10% oxygen in nitrogen. The oxidized spin-on dopant was stripped in 49% HF for 120 s. The sample was coated with 50 nm of SiO_2 by PECVD at 340 °C to prevent metal from contacting p-Si, and then windows to the n-wells were opened in SiO_2 by photolithography, followed by 30 s of oxygen plasma descum and 30 s of etching in 10:1 BOE. Photolithography and oxygen descum were used to define ribbons of p-n-p silicon, and then 10:1 BOE removed the oxide, a 30 s 20 W, 40 mTorr SF_6/Ar/O_2 plasma etch removed silicon down to the buried oxide, and the photoresist was removed. Metal contacts were deposited by dc sputtering using a quartz crystal monitor to measure the film thickness. Both top (source/drain) and back (gate) contacts were 150 nm Au with a 5 nm Cr adhesion layer. The contacts were patterned by photolithography, oxygen plasma descum, 25 min of etching in 10:1 DI H_2O/GE-6 gold etchant, and a 60 s dip in 4:1 DI H_2O/CR-12S chrome etchant. The contacts were annealed by RTA at 400 °C for 20 s in 8 s L/min forming gas (5%H_2/95%N_2). For the PMMA-coated devices, the top SiO_2 was removed by etching in 10:1 BOE and then 495K molecular weight PMMA diluted in anisole (roughly a 1.5% mixture by weight) was spin coated at 3000 rpm for 30 s and soft baked at 180 °C for 1 min. SiO_2 and PMMA thicknesses were monitored during processing by ellipsometry.

The mobility of these devices was estimated using a linear fit to $I_{DS}^{1/2}$ versus V_{GS} (Figure 5D) for the SiO_2-covered case, $\mu_{FET} = 2/C_{box}(\partial(I_{DS})^{1/2}/\partial V_{GS})^2 = 307$ cm^2 V^{-1} s^{-1}. For the PMMA-covered case, μ_{FET} after contact was found to be 125 cm^2 V^{-1} s^{-1}. We expect that the <1 order of magnitude difference in channel mobility is likely due to local chemical reactions at the p-Si/dielectric interface because PMMA was spin coated and SiO_2 was deposited by PECVD. An increased number of ionized traps in the PMMA case would explain the lower mobility.

■ ASSOCIATED CONTENT

Supporting Information. Force−distance setup and experimental XPS and AFM data. This material is available free of charge via the Internet at http://pubs.acs.org.

■ AUTHOR INFORMATION

Corresponding Author
*E-mail: hjacobs@umn.edu.

■ ACKNOWLEDGMENT

This research was partially supported by NSF CMMI-0755995 and CMMI-0621137.

■ REFERENCES

(1) Lowell, J.; Rose-Innes, A. C. *Adv. Phys.* **1980**, *29*, 947–1023.
(2) Duke, C. B.; Fabish, T. J. *Phys. Rev. Lett.* **1976**, *37*, 1075–1078.
(3) Horn, R. G.; Smith, D. T.; Grabbe, A. *Nature (London)* **1993**, *366*, 442–443.
(4) Xia, Y. N.; Whitesides, G. M. *Annu. Rev. Mater. Sci.* **1998**, *28*, 153–184.
(5) Loo, Y.-L.; Willett, R. L.; Baldwin, K. W.; Rogers, J. A. *J. Am. Chem. Soc.* **2002**, *124*, 7654–7655.
(6) Mesquida, P.; Stemmer, A. *Adv. Mater. (Weinheim, Ger.)* **2001**, *13*, 1395–1398.
(7) Jacobs, H. O.; Whitesides, G. M. *Science* **2001**, *291*, 1763–1766.
(8) Barry, C. R.; Steward, M. G.; Lwin, N. Z.; Jacobs, H. O. *Nanotechnology* **2003**, *14*, 1057–1063.
(9) Barry, C. R.; Lwin, N. Z.; Zheng, W.; Jacobs, H. O. *Appl. Phys. Lett.* **2003**, *83*, 5527.
(10) Barry, C. R.; Gu, J.; Jacobs, H. O. *Nano Lett.* **2005**, *5*, 2078–2084.
(11) As electrets, we tested poly(methyl methacrylate) (PMMA), poly(acrylic acid) (PAA), polystyrene (PS), MicroChem (SU-8) 2010 photoresist, and silicon dioxide (SiO_2). All polymers were spin-coated and baked according to standard procedures to produce thicknesses on the order of 100−200 nm except for the SU-8 resist, which was approximately 10 mm thick. The SiO_2 substrates (160 nm thick) were generated by dry thermal oxidation.
(12) Youn, B.-H.; Huh, C.-S. *Surf. Interface Anal.* **2003**, *35*, 445–449.
(13) Kim, H.-M.; Cho, Y.-H.; Lee, H.; Kim, S. I.; Ryu, S. R.; Kim, D. Y.; Kang, T. W.; Chung, K. S. *Nano Lett.* **2004**, *4*, 1059–1062.
(14) Bhattacharya, S.; Datta, A.; Berg, J. M.; Gangopadhyay, S. *J. Microelectromech. Syst.* **2005**, *14*, 590–597.
(15) Langowski, B. A.; Uhrich, K. E. *Langmuir* **2005**, *21*, 6366–6372.
(16) Jacobs, H. O.; Knapp, H. F.; Muller, S.; Stemmer, A. *Ultramicroscopy* **1997**, *69*, 39–49.

(17) XPS studies done by Uhrich et al. show small amounts of PDMS on the surface of plasma-treated PMMA after contact with plasma-treated PDMS but not on untreated PMMA.

(18) For a double layer separated by a distinct distance d, the charge density σ can be calculated with $\sigma = \varepsilon(\Delta V/d)$, where ε is the permittivity and ΔV is the voltage drop across the layer. For $\varepsilon = 2 \times 10^{-11}$ C/V m (relative permittivity of PMMA), $\Delta V = 2$ V (measured potential change), and $d = 200$ nm (assumed intermediate distance between the counter charges), we obtain a first-order estimate of the effective charge density of $\varepsilon_{\text{eff}} = 12.5$ elementary charges per surface area of 100 nm $\times$ 100 nm. The exact number depends on the actual distribution of the charges on the PMMA film and the Si substrate.

(19) The image charges flow from the ground through the electrometer into the metallic plates. A sufficient separation, >15 cm for 1 cm chips, between the two materials after contact ensures a correct charge reading. Accurate force−distance measurements required the disconnection of the electrometers before contact to eliminate any possible change in the plate charge due to electron flow associated with the image charges.

(20) Hillborg, H.; Gedde, U. W. *IEEE Trans. Dielectr. Electr. Insul.* **1999**, *6*, 703–717.

(21) Wainright, S. P.; Hall, S.; Flandre, D. *Solid-State Electron.* **1996**, *39*, 89–94.

(22) Casse, M.; Pretet, J.; Cristoloveanu, S.; Poiroux, T.; Fenouillet-Beranger, C.; Fruleux, F.; Raynaud, C.; Reimbold, G. *Solid-State Electron.* **2004**, *48*, 1243–1247.